


Article

Facile Synthesis of Phosphorus and Cobalt Co-Doped Graphitic Carbon Nitride for Fire and SmokeSuppressions of Polylactide Composite

Xianwu Cao ¹, Xiaoning Chi ¹, Xueqin Deng ¹, Qijun Sun ², Xianjing Gong ², Bin Yu ^{3,*}, Anthony Chun Yin Yuen ⁴ , Wei Wu ^{1,2,*} and Robert Kwow Yiu Li ²

- ¹ National Engineering Research Center of Novel Equipment for Polymer Processing, Key Laboratory of Polymer Processing Engineering of Ministry of Education, Guangdong Provincial Key Laboratory of Technique and Equipment for Macromolecular Advanced Manufacturing, South China University of Technology, Guangzhou 510640, China; ppeme@scut.edu.cn (X.C.); cxnxc0402@163.com (X.C.); xueqindd@163.com (X.D.)
- ² Department of Materials Science and Engineering, City University of Hong Kong, Tat Chee Avenue, Kowloon, Hong Kong SAR 999077, China; qjsun2-c@my.cityu.edu.hk (Q.S.); jingxgong2-c@my.cityu.edu.hk (X.G.); aprkyl@cityu.edu.hk (R.K.Y.L.)
- ³ Centre for Future Materials, University of Southern Queensland, Toowoomba 4350, Australia
- ⁴ School of Mechanical and Manufacturing Engineering, University of New South Wales, Sydney 2052, Australia; c.y.yuen@unsw.edu.au
- * Correspondence: bin.yu@usq.edu.au (B.Y.); weiwu39@scut.edu.cn (W.W.)

Received: 8 April 2020; Accepted: 6 May 2020; Published: 12 May 2020



Abstract: Due to the unique two-dimensional structure and features of graphitic carbon nitride ($g\text{-C}_3\text{N}_4$), such as high thermal stability and superior catalytic property, it is considered to be a promising flame retardant nano-additive for polymers. Here, we reported a facile strategy to prepare cobalt/phosphorus co-doped graphitic carbon nitride ($\text{Co/P-C}_3\text{N}_4$) by a simple and scalable thermal decomposition method. The structure of $\text{Co/P-C}_3\text{N}_4$ was confirmed by scanning electron microscopy (SEM), X-ray diffraction (XRD) and X-ray photoelectron spectroscopy (XPS). The carbon atoms in $g\text{-C}_3\text{N}_4$ were most likely substituted by phosphorous atoms. The thermal stability of polylactide (PLA) composites was increased continuously with increasing the content of $\text{Co/P-C}_3\text{N}_4$. In contrast to the $g\text{-C}_3\text{N}_4$, the Polylactide (PLA) composites containing $\text{Co/P-C}_3\text{N}_4$ exhibited better flame retardant efficiency and smoke suppression. With the addition of 10 wt % $\text{Co/P-C}_3\text{N}_4$, the peak heat release rate (PHRR), carbon dioxide (CO_2) production (PCO2P) and carbon oxide (CO) production (PCOP) values of PLA composites decreased by 22.4%, 16.2%, and 38.5%, respectively, compared to those of pure PLA, although the tensile strength of PLA composites had a slightly decrease. The char residues of $\text{Co/P-C}_3\text{N}_4$ composites had a more compact and continuous structure with few cracks. These improvements are ascribed to the physical barrier effect, as well as catalytic effects of $\text{Co/P-C}_3\text{N}_4$, which inhibit the rapid release of combustible gaseous products and suppression of toxic gases, i.e., CO.

Keywords: polylactide; graphitic carbon nitride; flame retardancy; smoke suppression

1. Introduction

Polylactide (PLA) is a widespread biobased and biodegradable polyester. It has been widely utilized in numerous fields, such as agriculture, packaging, automobile components and electronics [1–5], due to its superior physical and mechanical properties. However, some disadvantages, like poor thermal stability, weak mechanical strength and high flammability of PLA restrict its further applications.

Recently, two-dimensional (2D) nanomaterials such as graphene and its derivatives [6], montmorillonite (MMT) [7], and layered double hydroxide (LDH) [8,9], have been explored to improve the thermal stability, fire performance, and mechanical properties of PLA matrix.

Graphitic carbon nitride ($g\text{-C}_3\text{N}_4$) is a 2D nanomaterial that has received considerable attention, due to its thermal stability, chemical resistance and unique optical properties [10]. It can be large scale prepared by rapid polymerization of cheap precursors, like cyanamide [11], melamine [12], and dicyandiamide [13]. Nowadays, many researchers have attempted to utilize $g\text{-C}_3\text{N}_4$ or its modifications as flame-retardant additives to enhance the flame retardancy of polymers [14]. Shi et al. demonstrated that the $g\text{-C}_3\text{N}_4$ /MWCNT hybrid layer on the surface of PS spheres could act as "tortuous path" to reduce the permeation of heat [15]. The $g\text{-C}_3\text{N}_4$ nanosheets, in combination with reduced graphene oxide, served as excellent barriers in the PS matrix and reduced pyrolysis gaseous products during combustion [16]. Moreover, it has been demonstrated that the incorporation of various traditional flame retardants, together with $g\text{-C}_3\text{N}_4$, could endow polymers with better flame retardancy [17]. However, the poor thermal-oxidative stability and limited catalytic charring capacity of $g\text{-C}_3\text{N}_4$ limit its applications in flame retardation of polymeric materials. Element doping is considered as a convenient and effective method for adjusting the properties of $g\text{-C}_3\text{N}_4$ [18]. Different elements, including boron, phosphorus, sulfur, and cobalt have been introduced into the $g\text{-C}_3\text{N}_4$ framework successfully [19,20]. It is widely accepted that phosphorus-containing additives contribute to enhancing the flame retardancy of polymers [21,22]. Furthermore, it has been proved that the presence of transition metal elements perform good catalytic oxidation of CO and organic volatiles during combustion of polymers [23]. Therefore, it is reasonable to expect that the doped $g\text{-C}_3\text{N}_4$ with phosphorus and transition metal elements may possess good flame retardant performance for polymers. To the best of our knowledge, the application of doped $g\text{-C}_3\text{N}_4$ in flame retardant polymer materials with outstanding efficiency is still not reported.

In this work, cobalt/phosphorus co-doped $g\text{-C}_3\text{N}_4$ (Co/P- C_3N_4) was prepared by a simple and scalable thermal decomposition method. Then the effects of the Co/P- C_3N_4 concentration on thermal stability, fire safety and mechanical properties of PLA composites were studied. Meanwhile, the mechanism for fire hazard reduction of PLA was also proposed.

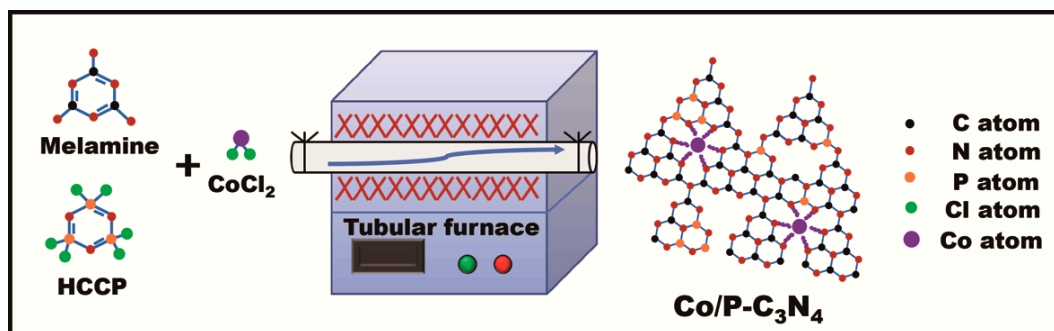
2. Materials and Methods

2.1. Materials

Poly lactide (PLA, Ingeo 4032D) was supplied by Natureworks (Minnetonka, MN, USA). Hexachlorotriphosphazene (HCCP), melamine, and cobalt chloride (CoCl_2) were purchased from J&K (Shanghai, China).

2.2. Preparation of Pure and Doped Graphitic Carbon Nitride

The pure and cobalt/phosphorus co-doped $g\text{-C}_3\text{N}_4$ (Co/P- C_3N_4) was prepared by one-step thermal decomposition method according to published work [24]. For pure graphitic carbon nitride ($g\text{-C}_3\text{N}_4$), the melamine was sealed a covered crucible and transformed into the tube furnace (OTF-1200X, Kejing Materials Technology Co, Hefei, China). A specimen was heated to 550 °C at a heating rate of 5 °C/min in air atmosphere, and maintained at 550 °C for 4 h to complete the reaction. For phosphorus and cobalt co-doped graphitic carbon nitride (Co/P- C_3N_4), the $\text{CoCl}_2 \cdot 6\text{H}_2\text{O}$ was first mixed with melamine in the weight ratio of 5/90, and dried in an air-circulating oven before grounding. Then, the HCCP was uniformly grounded and mixed with melamine and CoCl_2 . The weight ratio of HCCP and melamine was fixed at 1:9. Finally the sample was calcined as the same heating procedures. The synthesis diagram was shown in Scheme 1.



Scheme 1. The synthesis route of Co/P-C₃N₄.

2.3. Preparation of PLA-Based Composites

A desired amount of the obtained g-C₃N₄ or Co/P-C₃N₄ was mixed with PLA in an internal mixer (Plastic-Corder, Brabender, Duisburg, Germany). The samples were processed by setting at 190 °C, 60 rpm for 8 min. Then, pure PLA and PLA composites were molded into standard specimens for further characterization by hot-compression (190 °C, 5 min). The samples were abbreviated as g-C₃N₄-X and Co/P-C₃N₄-X, respectively, where X stands for the weight ratio of flame retardant fillers in PLA composites. The formulations were listed in Table 1.

Table 1. Formulations, LOI and UL-94 test results of PLA composites.

Samples	PLA (wt %)	g-C ₃ N ₄ (wt %)	Co/P-C ₃ N ₄ (wt %)	LOI (%)	UL-94 Test			
					t ₁ (s)	t ₂ (s)	UL-94 Rate	Dripping
Pure PLA	100	–	–	19.5	>50	–	NR	Yes
g-C ₃ N ₄ -2%	98	2	–	20	21.3	10.2	V-2	Yes
Co/P-C ₃ N ₄ -2%	98	–	2	21	15.8	20.4	V-2	Yes
Co/P-C ₃ N ₄ -5%	95	–	5	22	14.7	13.3	V-2	Yes
Co/P-C ₃ N ₄ -10%	90	–	10	22.5	12.8	3.5	V-1	Yes

2.4. Characterization

The morphology of the Co/P-C₃N₄ was observed by field-emission scanning electron microscopy (FE-SEM, Quanta 250, FEI, Waltham, MA, USA) with an energy-dispersive X-ray spectroscopy (EDX, Oxford Instrument, Abington, UK). Wide angle x-ray diffraction (XRD) patterns of the samples were recorded by using a X-Ray diffractometer (SmartLab, Rigaku, Tokyo, Japan) in the 2θ range of 10°–80° with a step of 0.02°. X-ray photoelectron spectroscopy (XPS, 5802 spectrometer, Physical Electronics PHI, Kanagawa, Japan) was used to determine the elemental compositions and chemical state of different elements. The melting enthalpies and recrystallization enthalpies were traced by a differential scanning calorimetry (DSC, DSC-204F1, Netzsch, Selb, Germany). Samples were heated and cooled in temperatures ranging from 30 to 190 °C at a ramp rate of 10 °C/min under nitrogen flow. Thermogravimetric analysis (TGA) was carried out on a thermal gravimetric analyzer (TGA-209F3, Netzsch, Selb, Germany) from 30 to 700 °C at a ramp rate of 10 °C/min under nitrogen flow. Limited oxygen index (LOI) testing was conducted on an oxygen index instrument (HC-2, Jiangning Analytical Instrument, Nanjing, China). The dimensions of the specimens were 100 × 6.5 × 3.0 mm³. The vertical burning test was carried out on a self-designed UL-94 vertical flame chamber according to GB/T2408-2008 with sample sizes measuring 130 × 13 × 3.0 mm³. Flammability properties were measured by a cone calorimeter (Fire Testing Technology, West Sussex, UK) according to the standard of ISO 5660. Samples (100 × 100 × 3 mm³) were tested under a heat flux of 35 kW/m².

3. Results and Discussion

3.1. Characterization of Co/P-C₃N₄

Figure 1a. shows the SEM image of the as-synthesized Co/P-C₃N₄. It is noted that the Co/P-C₃N₄ exhibits an aggregated, rough, and plate-like particles consisting of lamellar structures. The XRD patterns of the g-C₃N₄ and Co/P-C₃N₄ are presented in Figure 1b. It shows a strong diffraction peak at 27.7°, which is assigned to the (002) interplane of g-C₃N₄ induced by stacking of conjugated aromatic structures of thiotriazinone [25]. In addition, the peak located at 13.2° is ascribed to the diffraction of (100) plane. With the doping of cobalt (Co) and phosphorus (P) elements, the intensity of the diffraction peak at 43.1° and 57.4° decreases, suggesting that Co and P atoms have been doped into the structure of g-C₃N₄ successfully. To compare the thermal stability of g-C₃N₄ and Co/P-C₃N₄, TGA was performed under nitrogen atmosphere, as shown in Figure S1. It is obvious that the decomposition curve of Co/P-C₃N₄ shifts to a higher temperature, as compared with that of pure g-C₃N₄. Moreover, the residue at 800 °C for Co/P-C₃N₄ (6.68 wt %) is also higher than that of pure g-C₃N₄ (0.83 wt %). These results indicate that Co/P-C₃N₄ has a better thermal stability.

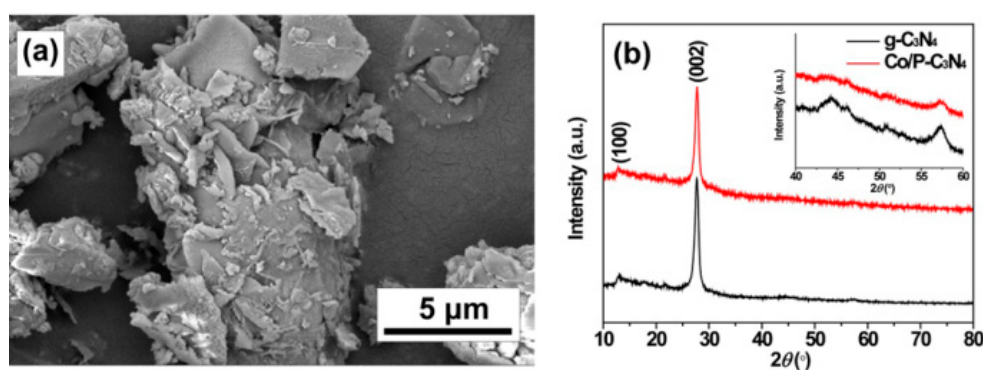


Figure 1. (a) SEM image of Co/P-C₃N₄, and (b) XRD patterns of g-C₃N₄ and Co/P-C₃N₄.

Figure 2a shows the XPS full survey spectra of g-C₃N₄ and Co/P-C₃N₄. It can be seen that there are three main peaks in the spectra, corresponding to C 1s, N 1s, and O 1s, respectively. The atomic percentage of carbon and nitrogen elements in Co/P-C₃N₄ decrease to 67.7 at.%, and 19.1 at.%, respectively, due to the introduction of cobalt and phosphorus. The presence of oxygen in g-C₃N₄ is due to the surface absorption and oxidation in air atmosphere, which is in good consistence with the reported results [24]. In addition, the oxygen content in Co/P-C₃N₄ increases significantly, compared with that of g-C₃N₄. It is conjectured that the Co/P element reacted with oxygen (O₂) in air atmosphere during the copolymerization reaction. The high resolution C 1s spectrum of g-C₃N₄ in Figure 2b shows three obvious peaks at 284.8, 286.2, and 288.1 eV, which are attributed to graphitic carbon (C–C), carbon in C–NH₂ species, and carbon in the N-containing aromatic ring (N–C=N), respectively [26,27]. With the doping of cobalt and phosphorus atoms, the N–C=N peak intensity for Co/P-C₃N₄ grows significantly, while the C–C peak intensity decreases simultaneously. In addition, the peak attributed to C–NH₂ bond disappears, indicating that the presence of Co and P atoms contributes to the polymerization of graphitic carbon nitride. The high resolution N 1s spectrum of g-C₃N₄ in Figure 2c can be deconvoluted into three peaks with the binding energy of 398.6, 399.2 and 400.6 eV. The main peak at 398.6 eV is attributed to the aromatic nitrogen in triazine rings (C–N=C), while two weak peaks located at 399.4 eV and 400.7 eV refer to the sp²-hybridized N bonds, i.e., [C–N(–C)–C] and C–N(–H)–C [28,29]. Moreover, the N 1s spectrum of Co/P-C₃N₄ exhibits three main deconvolution peaks at 398.4, 399.2 and 400.7 eV, showing a slight change after doping. The deconvoluted results of the N 1s spectra are shown in Table S1. It is observed that the atomic percentage of C–N=C groups for Co/P-C₃N₄ increases from 49.8% to 61.8%. As shown in Figure 2d, the signal peak centered at 132.7 eV in high resolution P 2p spectrum is ascribed to the P–N bond, while a weak band at 134.0 eV refers to the P=O bond,

which further confirm that the doped phosphorous atoms most likely substitute the carbon atoms in Co/P-C₃N₄ [30,31]. The characteristic peaks at 782.5 eV and 799.0 eV for Co 2p spectrum in Figure 2d correspond to Co 2p_{3/2} and Co 2p_{1/2}, respectively [32]. The above XPS results confirm the presence of Co and P elements, indicating the successful preparation of Co/P-C₃N₄.

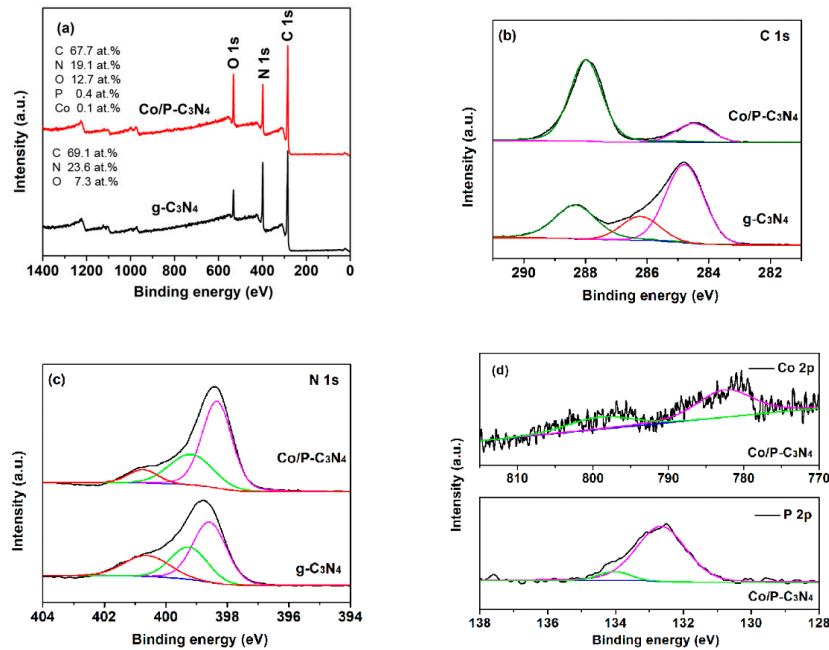


Figure 2. (a) XPS survey spectra, (b) C1s, (c) N1s, (d) P 2p and Co 2p of Co/P-C₃N₄.

3.2. Morphology of PLA Composites

Figure 3 presents the SEM images of the fractured surfaces for PLA composites. It is noted that pure PLA in Figure 3a has a smooth and no-crinkled surface, which is corresponding to the brittle fracture [33]. The fractured surface of PLA composites containing Co/P-C₃N₄ (Figure 3b–d) becomes rougher with increasing Co/P-C₃N₄. Furthermore, many tiny cavities could be found on the surfaces in Figure 3c,d, indicating that the poor interfacial interaction between Co/P-C₃N₄ and PLA matrix with a loading over a critical value.

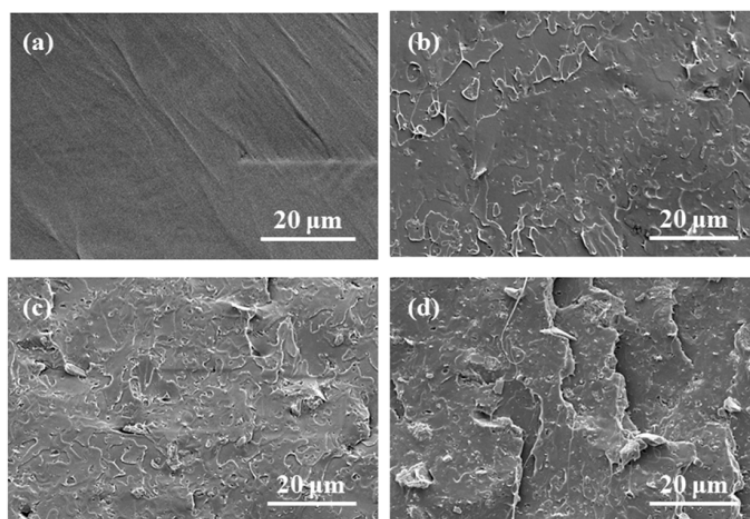


Figure 3. SEM images of pure PLA and PLA composites. (a) pure PLA, (b) Co/P-C₃N₄-2%, (c) Co/P-C₃N₄-5%, and (d) Co/P-C₃N₄-10%.

3.3. Crystallization Behavior of PLA Composites

The crystallization behavior of PLA composites was measured by DSC. Figure 4 depicts the first cooling and second heating curves of PLA composites as a function of Co/P-C₃N₄ content. As shown in Figure 4a, no crystallization peaks appear during the cooling process, which is caused by the rigid segments in the PLA main chain [34]. As shown in Table 2, the glass transition temperature (*T_g*) of the PLA composites are higher than that of pure PLA, which suggests that the introduction of Co/P-C₃N₄ hinders the movement of the PLA segments. The exothermic peaks observed between 100 and 130 °C in Figure 4b are associated with the cold crystallization of PLA. In addition, it is noted that double endothermic peaks appear around 170 °C in the Co/P-C₃N₄ composites, which are related to the melting of PLA. Fukushima et al. reported that the melt-recrystallization phenomenon of PLA was ascribed to different forms of crystals [35]. The low-melting peak (*T_{m1}*) relates to the β-crystal, which is an imperfect crystal structure, while the high-melting peak (*T_{m2}*) is assigned to the most common polymorph α-crystal of PLA. This result indicates that the addition of Co/P-C₃N₄ will restrict the mobility of PLA chains, which is similar to other PLA-based composites [36]. The cold-crystallization enthalpy (ΔH_{cc}) of Co/P-C₃N₄-2% shows a little increase as compared with that of pure PLA. With further increasing the content of Co/P-C₃N₄, ΔH_{cc} decreases significantly. Similarly, the melting enthalpies (ΔH_m) exhibit a decrease trend with the filler content. In addition, the crystallinity degree (χ_c) of PLA composites is lower than that of pure PLA, indicating that Co/P-C₃N₄ has no nucleation effect on PLA matrix [37].

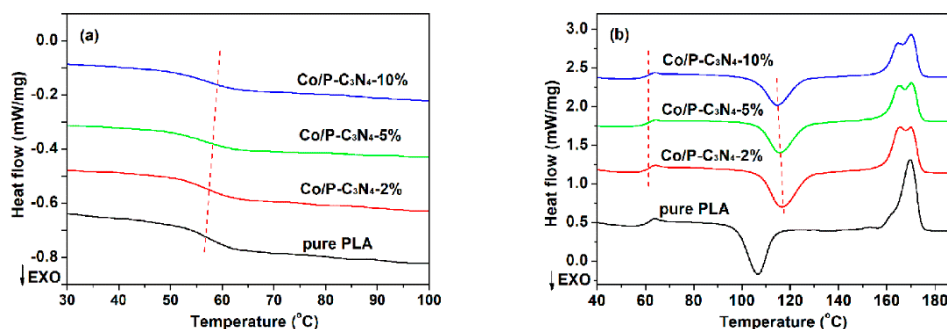


Figure 4. DSC curves of pure PLA and PLA composites. (a) First cooling, (b) second heating.

Table 2. DSC data of PLA composites.

Samples	<i>T_g</i> (°C)	<i>T_{cc}</i> (°C)	ΔH_{cc} (J/g)	<i>T_{m1}</i> (°C)	<i>T_{m2}</i> (°C)	ΔH_m (J/g)	χ_c (%)
Pure PLA	61.5	106.5	35.5	–	169.6	41.2	6.1
Co/P-C ₃ N ₄ -2%	62.1	116.5	36.0	165.6	169.7	38.9	3.2
Co/P-C ₃ N ₄ -5%	62.2	115.7	28.6	165.3	170.1	31.8	3.6
Co/P-C ₃ N ₄ -10%	62.3	114.7	27.3	165.1	170.0	31.3	4.6

3.4. Thermal Stability of PLA Composites

The thermal stability of PLA composites under nitrogen atmosphere were examined with the detailed results shown in Figure 5 and Table 3. *T₁₀* represents the initial decomposition temperature where 10% weight loss occurs, while *T_{max}* refers to the temperature at the maximum mass loss rate. As shown in Figure 5a, the *T₁₀* values are 338.1, 339.8 and 342.8 °C for Co/P-C₃N₄-2%, Co/P-C₃N₄-5% and Co/P-C₃N₄-10%, respectively, which are all slightly higher than that of pure PLA (335.1 °C). This phenomenon may be ascribed to the labyrinth effect of Co/P-C₃N₄ in the composites [38]. From Figure 5b, it is observed that pure PLA shows only one peak between 300 and 380 °C, which is ascribed to the chain scission of PLA. Two decomposition peaks are observed for PLA composites. The main peak in the temperature range of 300–400 °C is similar to pure PLA, while the small peak between 500 and 650 °C corresponds to the decomposition of Co/P-C₃N₄. This is due to the thermal decomposition of Co/P-C₃N₄ at a higher temperature. As shown in Table 3, pure PLA shows almost

no char residues at 700 °C. whereas the char residues of PLA composites increase continuously with increasing Co/P-C₃N₄ content, which are attributed to the catalytic charring capability of Co/P-C₃N₄.

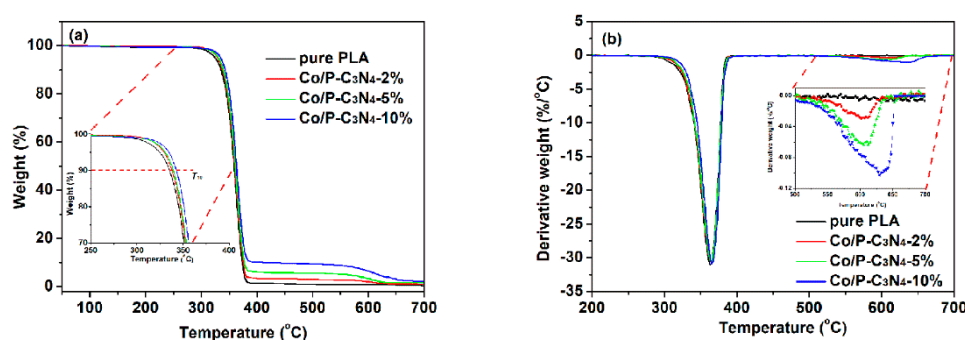


Figure 5. (a) TGA, and (b) DTG curves of PLA composites under nitrogen atmosphere.

Table 3. TGA data of PLA composites.

Samples	T_{10} (°C)	T_{max} (°C)	Char Residue at 700 °C (wt %)
Pure PLA	335.6	364.9	0.03
Co/P-C ₃ N ₄ -2%	338.1	365.2	1.65
Co/P-C ₃ N ₄ -5%	339.8	364.9	1.78
Co/P-C ₃ N ₄ -10%	342.8	365.8	1.96

3.5. Fire Performance of PLA Composites

LOI and UL-94 vertical burning tests are widely utilized to assess the flame retardant performance of polymers for specific engineering applications. The LOI and UL-94 test results for pure PLA and its composites are presented in Table 1. Pure PLA has a lower LOI value of 19.5% and no rating in UL-94 test, indicating it is highly susceptible to flames. The LOI values of PLA composites exhibit a slightly increase with the addition of Co/P-C₃N₄. Moreover, the presence of Co/P-C₃N₄ had a positive effect on the UL-94 vertical burning tests. The samples of PLA composite containing 10 wt % Co/P-C₃N₄ exhibit a reduced burning rate and pass V-1 rating, which is much better than those of pure PLA. However, the dripping phenomenon of PLA is still persisted.

Cone calorimetry is one of the most comprehensive methods to measure the combustion performance of polymer materials [39–41]. The heat release rate (HRR), total heat release (THR), carbon dioxide (CO₂) production rate (CO₂P) and carbon monoxide (CO) production rate (COP) curves of pure PLA and its composites are shown in Figure 6, and the corresponding data are listed in Table 4. In Figure 6a, the peak of HRR (pHRR) of g-C₃N₄-2% reduces to 364.8 kW/m² showing a slight decrease, compared with that of pure PLA (394.3 kW/m²). This is due to the fact that g-C₃N₄ serves as a thermal barrier to reduce rapid heat release during combustion [42]. In the case of Co/P-C₃N₄-2%, the pHRR value decreases to 321.0 kW/m², indicating that Co/P-C₃N₄ exhibits a better barrier effect than g-C₃N₄. Moreover, a significant delay in time to ignition (TTI) is observed for PLA-Co/P-C₃N₄ composites. Particularly, the maximum delay is observed for Co/P-C₃N₄-10% (~79 s). The THR curves of pure PLA and PLA composites are presented in Figure 6b. It is evident that the THR of PLA composites containing Co/P-C₃N₄ decreases continuously with the increase of Co/P-C₃N₄ content. For instance, the THR value of Co/P-C₃N₄-10% decreases from 56.4 to 51.9 MJ/m². Toxic gases and fumes are regarded as larger threatens during fire accident [43]. The CO₂ production rate (CO₂P) curves of pure PLA and its composites are depicted in Figure 6c. It is observed that the CO₂P exhibits a similar tendency to HRR value. The peak CO₂ production rate (PCO₂P) for Co/P-C₃N₄-10% decreases to 0.390 g/s, which is reduced by 16.2%, as compared to that of pure PLA. It is worthy to note that the peak of CO production rate (PCOP) of g-C₃N₄-2% increases up to 504.7 ppm (Figure 6d). It is speculated that the introduction of pure g-C₃N₄ isolates oxygen, resulting in the incomplete combustion of PLA matrix. In comparison, the presence of Co/P-C₃N₄ can inhibit the production rate of CO. With the

incorporation of 10 wt % Co/P-C₃N₄, the PCOP value reduces noticeably by 38.5% compared to pure PLA (174.9 ppm). Co atoms can play a catalytic role during combustion and convert toxic gases such as CO into non-toxic gases, which is very conducive to evacuation in a fire [44,45].

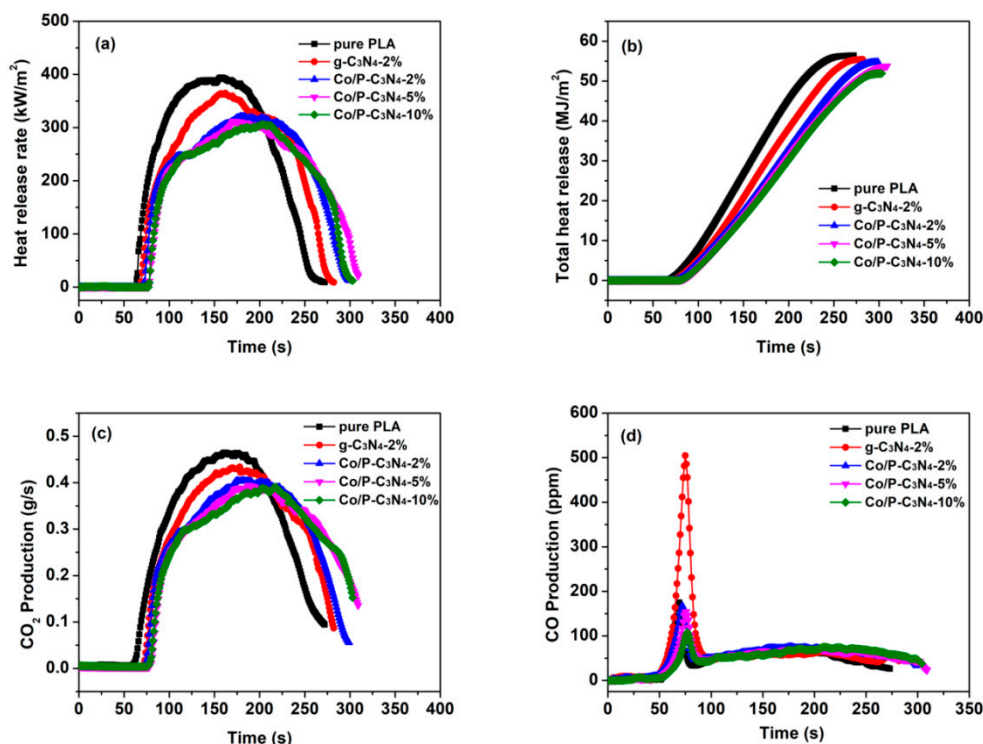


Figure 6. Cone calorimeter test results of pure PLA and PLA composites: (a) heat release rates, (b) total heat release, (c) CO₂ production rate, and (d) CO production rate as a function of time.

Table 4. Combustion results of control PLA and its composites obtained from cone calorimeter tests.

Samples	TTI (s)	T _{PHRR} (s)	PHRR (kW/m ²)	THR (MJ/m ²)	Char Residue (wt %)	PCO ₂ P (g/s)	PCOP (ppm)
Pure PLA	63	158	394.3	56.4	0.1	0.465	174.9
g-C ₃ N ₄ -2%	69	162	364.8	55.4	3.9	0.434	504.7
Co/P-C ₃ N ₄ -2%	73	180	321.0	54.7	5.5	0.405	168.0
Co/P-C ₃ N ₄ -5%	78	176	311.9	53.8	7.1	0.394	154.3
Co/P-C ₃ N ₄ -10%	79	204	306.1	51.9	8.9	0.390	107.6

3.6. Analysis of Char Residues

Digital photos of char residues are reported in Figure 7. Almost no char residues can be observed for control PLA, as shown in Figure 7a, indicating that pure PLA is completely burnt out. With the addition of 2 wt % g-C₃N₄, the char residues exhibit many cracks and unintegrated structure (Figure 7b). Meanwhile, the PLA composites containing Co/P-C₃N₄ (Figure 7c–e) have thick, integrated, and dense carbonization zone. With increasing the Co/P-C₃N₄ content, the char layer becomes thicker which is favorable for preventing heat conduction and gas diffusion to inhibit the combustion [46]. To observe the micromorphology of the char residues, the SEM images are presented in Figure 8. Figure 8a shows that the char residues of g-C₃N₄-2% exhibit a loose and porous structure with a large number of honeycomb piles-like pores, which cannot hinder the burning efficiently. For Co/P-C₃N₄-2% (Figure 8b), the compact and continuous char layer can be observed, suggesting that the char-forming process is improved. The presence of Co and P elements in doped g-C₃N₄ contributes to the formation of intact char residues to hinder heat transfer and slow down the diffusion of gas during combustion.

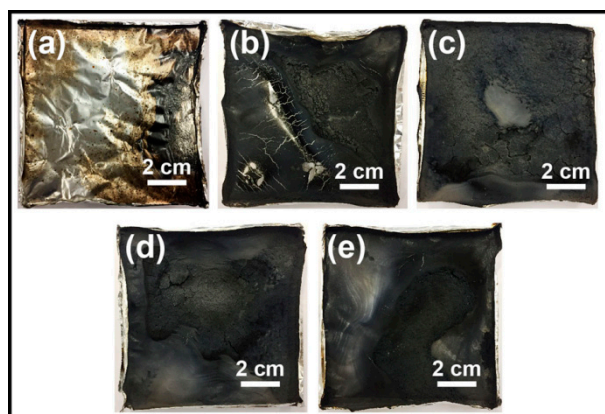


Figure 7. Digital photos of char residues after cone calorimeter tests: (a) pure PLA, (b) $g\text{-C}_3\text{N}_4\text{-2\%}$, (c) $\text{Co/P-C}_3\text{N}_4\text{-2\%}$, (d) $\text{Co/P-C}_3\text{N}_4\text{-5\%}$, and (e) $\text{Co/P-C}_3\text{N}_4\text{-10\%}$.

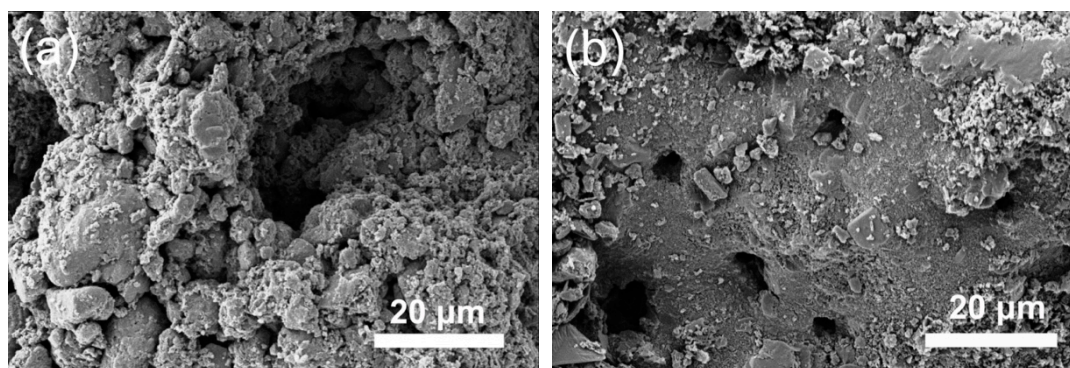


Figure 8. SEM images of char residues (a) $g\text{-C}_3\text{N}_4\text{-2\%}$, and (b) $\text{Co/P-C}_3\text{N}_4\text{-2\%}$.

The chemical composition of char residues was examined by XPS, and the relevant results are shown in Figure 9 and Table S2. It is observed that the high resolution C 1s spectrum of $g\text{-C}_3\text{N}_4\text{-2\%}$ in Figure 9a can be deconvoluted into three peaks at 287.4, 284.8 and 283.9 eV, corresponding to C=O, C–C and graphitic C–C, respectively. As shown in Figure 9b, the deconvoluted peaks at 287.6, 284.4 and 283.8 eV for C 1s spectrum are assigned to C=O/C–P, C–C and graphitic C–C. As observed in Table S2, the atomic percentage of graphitic C in the char residues of $\text{Co/P-C}_3\text{N}_4\text{-2\%}$ decreases from 17.8% to 7.1% for $g\text{-C}_3\text{N}_4\text{-2\%}$. Meanwhile, the atomic ratio of C=O and/or C–P bonds increases from 70.4% to 79%. The N 1s spectra (Figure 9c,d) of the char residues for $g\text{-C}_3\text{N}_4\text{-2\%}$ and $\text{Co/P-C}_3\text{N}_4\text{-2\%}$ are fitted to three similar peaks. The percentage of O–N=O bonds (397.9 eV) in the char residue of $\text{Co/P-C}_3\text{N}_4\text{-2\%}$ is 65.7%, which is higher than that of $g\text{-C}_3\text{N}_4\text{-2\%}$ (53.2%). Moreover, the high-resolution spectrum of P 2p in Figure 9e indicates the coexistence of P–C (133.8 eV), O–P=O (132.8 eV) and P–O–P (132.1 eV). Such char layer is believed to serve as a better physical barrier in protecting the underlying polymers against a flame [47–49].

Based on the abovementioned analysis, the possible flame retardant mechanism is illustrated in Figure 10. Pure PLA absorbs heat and releases volatile gaseous without any restriction upon exposure to a fire. It will release a large amount of smoke and toxic gases (CO) due to continuous fuel supply, which will increase the potential fire hazard of PLA. With the addition of $g\text{-C}_3\text{N}_4$, PLA composites can form a loose and discontinuous char layer with many cracks. The heat and oxygen can penetrate into this char layer easily, resulting in a low protection efficiency for underlying polymers [50]. Noticeably, the CO production rate of PLA/ $g\text{-C}_3\text{N}_4$ composite increases significantly as compared to that of pure PLA. It is conjectured that the char layer isolates oxygen and fuel, resulting in the incomplete combustion of PLA. As a comparison, the char residue of PLA composite containing $\text{Co/P-C}_3\text{N}_4$ shows a compact and coherent structure. In addition, P/Co co-doped $\text{-C}_3\text{N}_4$ generates more active sites with

high catalytic capability in addition to catalytic role of Coin char layer, which contributes to oxidation of the toxic pyrolysis product, i.e., CO into CO₂ [51].

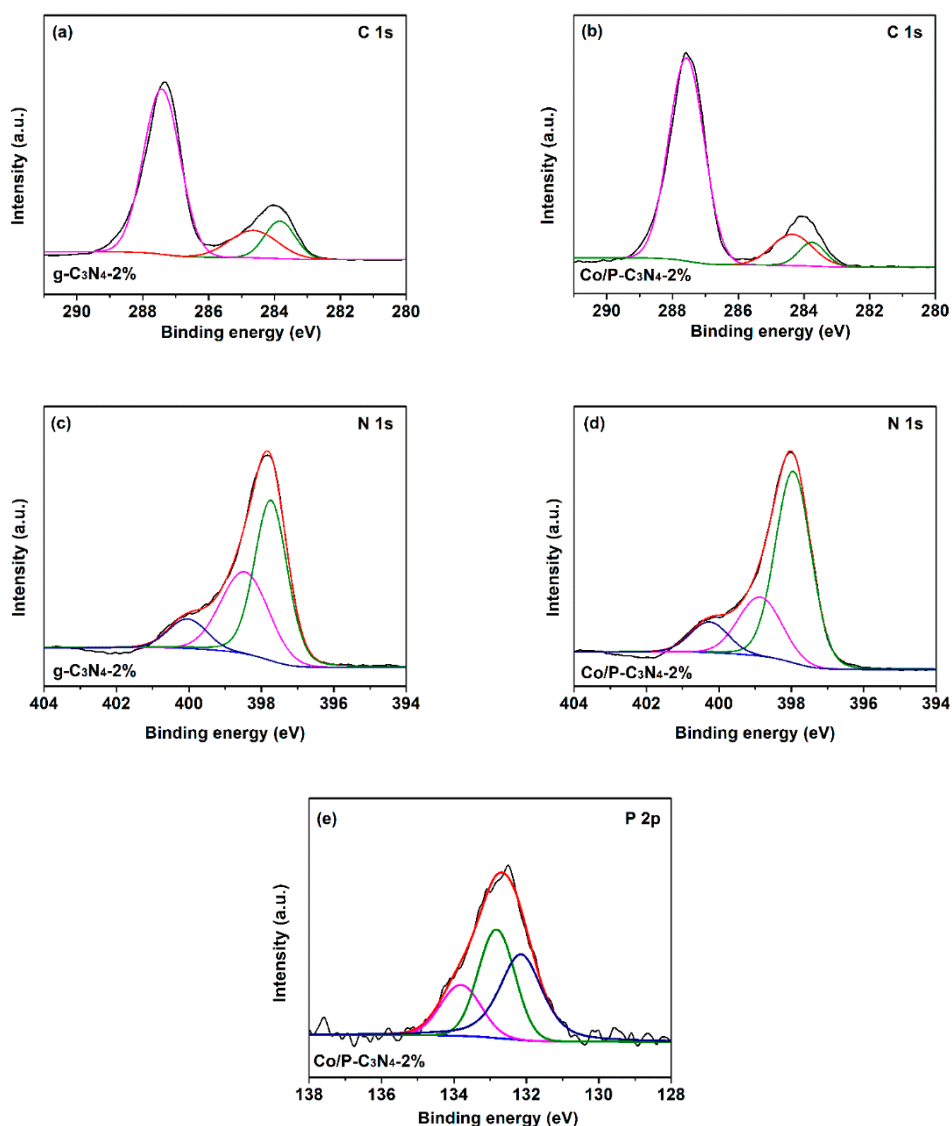


Figure 9. High resolution XPS spectra of char residues. (a) C 1s, and (c) N 1s, of g-C₃N₄, (b) C 1s, (d) N 1s, and (e) P 2p, of Co/P-C₃N₄.

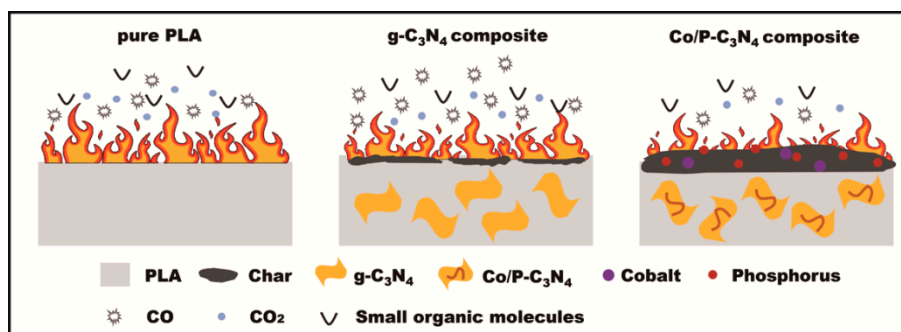


Figure 10. Schematic diagram of flame retardant mechanism of PLA composites.

3.7. Mechanical Properties

The tensile stress-strain curves of PLA composites are shown in Figure 11a. It is observed that both the tensile strength and elongation at the break of the PLA composites decrease continuously as compared with those of pure PLA. The higher loading of the Co/P-C₃N₄ results in larger Young's modulus and smaller elongation at break. It can be explained that the Co/P-C₃N₄ serves as a rigid filler to restrict the movement of PLA molecular chains and bear the force themselves [52,53]. However, the poor interface adhesion between Co/P-C₃N₄ and PLA, as shown in Figure 3, will lead to a decrease in tensile strength. Figure 11b presents the dependence of tensile strength and Young's modulus of PLA composites on Co/P-C₃N₄ content. It is found that pure PLA belongs to a brittle material with a tensile strength of 58.05 MPa and a Young's modulus of 1349 MPa. With the addition of 10 wt % Co/P-C₃N₄, the tensile strength of PLA composites decreases to 50.21 MPa. Meanwhile, the Young's modulus of Co/P-C₃N₄-10% reaches 1496 MPa, a 10.9% improvement, compared with that of pure PLA.

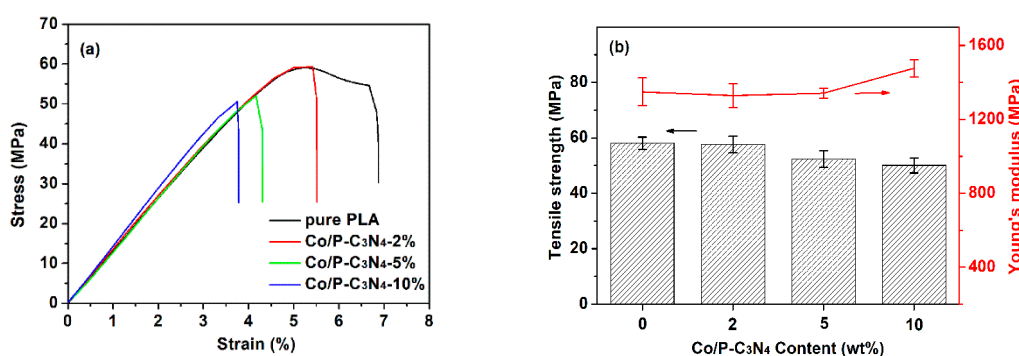


Figure 11. (a) Typical stress-strain curves, (b) tensile properties of pure PLA and PLA composites.

4. Conclusions

In this work, we demonstrated a facile strategy to prepare Co/P-C₃N₄ by a simple and scalable thermal decomposition method, which was then utilized to prepare flame retardant PLA composites. The structure of Co/P-C₃N₄ was confirmed by SEM, XRD and XPS. Then, the effects of Co/P-C₃N₄ concentration on crystallization behavior, thermal stability, fire performance and mechanical properties of PLA were investigated. The results revealed that Co/P-C₃N₄ could restrict the mobility of PLA chains to some extent. The thermal stability of PLA composites was increased continuously with increasing the content of Co/P-C₃N₄. The PLA composite containing 10 wt % Co/P-C₃N₄ exhibited better fire resistance with a moderate decrease in PHRR, PCO₂P and PCOP values, by 22.4%, 16.2%, and 38.5%, respectively. In addition, the analysis of char residues revealed that the addition of Co/P-C₃N₄ contributed to the formation of protective char layer with compact and continuous structure. These improvements in thermal stability and fire retardation of PLA can be ascribed to the physical barrier effect, as well as catalytic effects of Co/P-C₃N₄. Furthermore, the introduction of Co/P-C₃N₄ resulted in a slight decrease in tensile strength as compared to pure PLA.

Supplementary Materials: The following are available online at <http://www.mdpi.com/2073-4360/12/5/1106/s1>, Figure S1: TGA curves of g-C₃N₄ and Co-C₃N₄ at a heating rate of 10 °C/min under nitrogen atmosphere. Table S1: Deconvoluted results of the XPS N 1s spectra of g-C₃N₄ and Co/P-C₃N₄. Table S2: XPS Fitting results of char residues.

Author Contributions: Investigation, X.C. (Xiaoning Chi), X.D., Q.S., X.G., and A.C.Y.Y.; writing—original draft preparation, W.W., and B.Y.; methodology, W.W. and X.C. (Xianwu Cao); writing—review and editing, R.K.Y.L.; supervision, X.C. (Xianwu Cao), and R.K.Y.L.; All authors have read and agreed to the published version of the manuscript.

Funding: This research was funded by National Key Research and Development Program of China (Grant number 2016YFB0302000), Fundamental Research Funds for the Central Universities of China (Grant number 2019MS062), National Natural Science Foundation of China (Grant number 51803029), Australian Research Council Discovery Early Career Research Award (Grant number DE190101176), Australian Research Council Industrial Training Transformation Centre (Grant number IC170100032), and City University of Hong Kong (Grant number 9678103).

Conflicts of Interest: The authors declare no conflict of interest.

References

1. Vink, E.T.H.; Rabago, K.R.; Glassner, D.A.; Springs, B.; O'Connor, R.P.; Kolstad, J.; Gruber, P.R. The sustainability of NatureWorks (TM) polylactide polymers and Ingeo (TM) polylactide fibers(a): An update of the future. *Macromol. Biosci.* **2004**, *4*, 551–564. [[CrossRef](#)]
2. Wu, W.; Han, S.T.; Venkatesh, S.; Sun, Q.J.; Peng, H.Y.; Zhou, Y.; Yeung, C.C.; Li, R.K.Y.; Roy, V.A.L. Biodegradable skin-Inspired nonvolatile resistive switching memory based on gold nanoparticles embedded alkali lignin. *Org. Electron.* **2018**, *59*, 382–388. [[CrossRef](#)]
3. Tawiah, B.; Yu, B.; Wei, R.C.; Yuen, R.K.K.; Chen, W.; Xin, J.H.; Fei, B. Simultaneous fire safety enhancement and mechanical reinforcement of poly (lactic acid) biocomposites with hexaphenyl (nitrilotris(ethane-2,1-diy))tris (phosphoramidate). *J. Hazard. Mater.* **2019**, *380*, 120856. [[CrossRef](#)]
4. Mayekar, P.C.; Castro-Aguirre, E.; Auras, R.; Selke, S.; Narayan, R. Effect of nano-Clay and surfactant on the biodegradation of poly(lactic acid) Films. *Polymers* **2020**, *12*, 311. [[CrossRef](#)]
5. Tarres, Q.; Oliver-Ortega, H.; Espinach, F.X.; Mutje, P.; Delgado-Aguilar, M.; Mendez, J.A. Determination of mean intrinsic flexural strength and coupling factor of natural fiber reinforcement in polylactic acid biocomposites. *Polymers* **2019**, *11*, 1736. [[CrossRef](#)] [[PubMed](#)]
6. Jing, J.; Zhang, Y.; Fang, Z.P.; Wang, D.Y. Core-Shell flame retardant/graphene oxide hybrid: A self-Assembly strategy towards reducing fire hazard and improving toughness of polylactic acid. *Compos. Sci. Technol.* **2018**, *165*, 161–167. [[CrossRef](#)]
7. Cheng, K.C.; Yu, C.B.; Guo, W.J.; Wang, S.F.; Chuang, T.H.; Lin, Y.H. Thermal properties and flammability of polylactide nanocomposites with aluminum trihydrate and organoclay. *Carbohydr. Polym.* **2012**, *87*, 1119–1123. [[CrossRef](#)]
8. Zhang, S.; Yan, Y.X.; Wang, W.J.; Gu, X.Y.; Li, H.F.; Li, J.H.; Sun, J. Intercalation of phosphotungstic acid into layered double hydroxides by reconstruction method and its application in intumescent flame retardant poly (lactic acid) composites. *Polym. Degrad. Stabil.* **2018**, *147*, 142–150. [[CrossRef](#)]
9. Tawiah, B.; Yu, B.; Fei, B. Advances in Flame Retardant Poly(Lactic Acid). *Polymers* **2018**, *10*, 876. [[CrossRef](#)]
10. Liu, J.; Wang, H.; Antonietti, M. Graphitic carbon nitride “reloaded”: Emerging applications beyond (photo) catalysis. *Chem. Soc. Rev.* **2016**, *45*, 2308–2326. [[CrossRef](#)]
11. Lau, V.W.H.; Moudrakovski, I.; Botari, T.; Weinberger, S.; Mesch, M.B.; Duppel, V.; Senker, J.; Blum, V.; Lotsch, B.V. Rational design of carbon nitride photocatalysts by identification of cyanamide defects as catalytically relevant sites. *Nat. Commun.* **2016**, *7*, 12165. [[CrossRef](#)] [[PubMed](#)]
12. Chen, Z.; Yu, X.; Zhu, Q.H.; Fan, T.T.; Wu, Q.L.; Zhang, L.Z.; Li, J.H.; Fang, W.P.; Yi, X.D. Steam engraving optimization of graphitic carbon nitride with enhanced photocatalytic hydrogen evolution. *Carbon* **2018**, *139*, 189–194. [[CrossRef](#)]
13. Cheng, J.S.; Hu, Z.; Lv, K.L.; Wu, X.F.; Li, Q.; Li, Y.H.; Li, X.F.; Sun, J. Drastic promoting the visible photoreactivity of layered carbon nitride by polymerization of dicyandiamide at high pressure. *Appl. Catal. B Environ.* **2018**, *232*, 330–339. [[CrossRef](#)]
14. Shi, Y.Q.; Wang, L.C.; Fu, L.B.; Liu, C.; Yu, B.; Yang, F.Q.; Hu, Y. Sodium alginate-Templated synthesis of g-C₃N₄/carbon spheres/Cu ternary nanohybrids for fire safety application. *J. Colloid Interf. Sci.* **2019**, *539*, 1–10. [[CrossRef](#)] [[PubMed](#)]
15. Shi, Y.Q.; Long, Z.; Yu, B.; Zhou, K.Q.; Gui, Z.; Yuen, R.K.K.; Hu, Y. Tunable thermal, flame retardant and toxic effluent suppression properties of polystyrene based on alternating graphitic carbon nitride and multi-walled carbon nanotubes. *J. Mater. Chem. A* **2015**, *3*, 17064–17073. [[CrossRef](#)]
16. Shi, Y.Q.; Liu, C.; Fu, L.B.; Yang, F.Q.; Lv, Y.C.; Yu, B. Hierarchical assembly of polystyrene/graphitic carbon nitride/reduced graphene oxide nanocomposites toward high fire safety. *Compos. Part B Eng.* **2019**, *179*, 107541. [[CrossRef](#)]
17. Shi, Y.Q.; Yu, B.; Duan, L.J.; Gui, Z.; Wang, B.B.; Hu, Y.; Yuen, R.K.K. Graphitic carbon nitride/phosphorus-rich aluminum phosphinates hybrids as smoke suppressants and flame retardants for polystyrene. *J. Hazard. Mater.* **2017**, *332*, 87–96. [[CrossRef](#)]
18. Jiang, L.B.; Yuan, X.Z.; Pan, Y.; Liang, J.; Zeng, G.M.; Wu, Z.B.; Wang, H. Doping of graphitic carbon nitride for photocatalysis: A review. *Appl. Catal. B Environ.* **2017**, *217*, 388–406. [[CrossRef](#)]

19. Chen, D.D.; Liu, J.G.; Jia, Z.Z.; Fang, J.Z.; Yang, F.; Tang, Y.M.; Wu, K.; Liu, Z.; Fang, Z.Q. Efficient visible-Light-Driven hydrogen evolution and Cr(VI) reduction over porous P and Mo co-doped g-C₃N₄ with feeble N vacancies photocatalyst. *J. Hazard. Mater.* **2019**, *361*, 294–304. [[CrossRef](#)]
20. Wang, K.Y.; Gu, G.Z.; Hu, S.Z.; Zhang, J.; Sun, X.L.; Wang, F.; Li, P.; Zhao, Y.F.; Fan, Z.P.; Zou, X. Molten salt assistant synthesis of three-Dimensional cobalt doped graphitic carbon nitride for photocatalytic N₂ fixation: Experiment and DFT simulation analysis. *Chem. Eng. J.* **2019**, *368*, 896–904. [[CrossRef](#)]
21. Rao, W.H.; Liao, W.; Wang, H.; Zhao, H.B.; Wang, Y.Z. Flame-Retardant and smoke-Suppressant flexible polyurethane foams based on reactive phosphorus-containing polyol and expandable graphite. *J. Hazard. Mater.* **2018**, *360*, 651–660. [[CrossRef](#)] [[PubMed](#)]
22. Shi, Y.Q.; Yu, B.; Zheng, Y.Y.; Yang, J.; Duan, Z.P.; Hu, Y. Design of reduced graphene oxide decorated with DOPO-phosphanomidate for enhanced fire safety of epoxy resin. *J. Colloid Interf. Sci.* **2018**, *521*, 160–171. [[CrossRef](#)] [[PubMed](#)]
23. Xu, W.Z.; Wang, X.L.; Wu, Y.; Li, W.; Chen, C.Y. Functionalized graphene with Co-ZIF adsorbed borate ions as an effective flame retardant and smoke suppression agent for epoxy resin. *J. Hazard. Mater.* **2019**, *363*, 138–151. [[CrossRef](#)] [[PubMed](#)]
24. Li, X.F.; Zhang, J.; Shen, L.H.; Ma, Y.M.; Lei, W.W.; Cui, Q.L.; Zou, G.T. Preparation and characterization of graphitic carbon nitride through pyrolysis of melamine. *Appl. Phys. A Mater.* **2009**, *94*, 387–392. [[CrossRef](#)]
25. Zhao, Y.C.; Yu, D.L.; Zhou, H.W.; Tian, Y.J.; Yanagisawa, O. Turbostratic carbon nitride prepared by pyrolysis of melamine. *J. Mater. Sci.* **2005**, *40*, 2645–2647. [[CrossRef](#)]
26. Zhu, Y.P.; Ren, T.Z.; Yuan, Z.Y. Mesoporous phosphorus-Doped g-C₃N₄ nanostructured flowers with superior photocatalytic hydrogen evolution performance. *ACS Appl. Mater. Inter.* **2015**, *7*, 16850–16856. [[CrossRef](#)]
27. Gu, S.; Xie, J.L.; Li, C.M. Hierarchically porous graphitic carbon nitride: Large-Scale facile synthesis and its application toward photocatalytic dye degradation. *RSC Adv.* **2014**, *4*, 59436–59439. [[CrossRef](#)]
28. Zhou, Y.J.; Zhang, L.X.; Liu, J.J.; Fan, X.Q.; Wang, B.Z.; Wang, M.; Ren, W.C.; Wang, J.; Li, M.L.; Shi, J.L. Brand new P-doped g-C₃N₄: Enhanced photocatalytic activity for H₂ evolution and Rhodamine B degradation under visible light. *J. Mater. Chem. A* **2015**, *3*, 3862–3867. [[CrossRef](#)]
29. Wang, B.; Yin, X.H.; Peng, D.; Lv, R.H.; Na, B.; Liu, H.S.; Gu, X.B.; Wu, W.; Zhou, J.L.; Zhang, Y. Achieving thermally conductive low loss PVDF-based dielectric composites via surface functionalization and orientation of SiC nanowires. *Express Polym. Lett.* **2020**, *14*, 2–11. [[CrossRef](#)]
30. Zhang, Y.J.; Mori, T.; Ye, J.H.; Antonietti, M. Phosphorus-Doped carbon nitride solid: Enhanced electrical conductivity and photocurrent generation. *J. Am. Chem. Soc.* **2010**, *132*, 6294–6295. [[CrossRef](#)]
31. Lan, D.H.; Wang, H.T.; Chen, L.; Au, C.T.; Yin, S.F. Phosphorous-Modified bulk graphitic carbon nitride: Facile preparation and application as an acid-Base bifunctional and efficient catalyst for CO₂ cycloaddition with epoxides. *Carbon* **2016**, *100*, 81–89. [[CrossRef](#)]
32. Chen, P.W.; Li, K.; Yu, Y.X.; Zhang, W.D. Cobalt-Doped graphitic carbon nitride photocatalysts with high activity for hydrogen evolution. *Appl. Surf. Sci.* **2017**, *392*, 608–615. [[CrossRef](#)]
33. Wu, W.; Cao, X.W.; Zhang, Y.J.; He, G.J. Polylactide/halloysite nanotube nanocomposites: Thermal, mechanical properties, and foam processing. *J. Appl. Polym. Sci.* **2013**, *130*, 443–452. [[CrossRef](#)]
34. Wu, W.; Liu, T.; Zhang, D.L.; Sun, Q.J.; Cao, K.; Zha, J.W.; Lu, Y.; Wang, B.; Cao, X.W.; Feng, Y.H.; et al. Significantly improved dielectric properties of polylactide nanocomposites via TiO₂ decorated carbon nanotubes. *Compos. Part A Appl. S.* **2019**, *127*, 105650. [[CrossRef](#)]
35. Fukushima, K.; Tabuani, D.; Arena, M.; Gennari, M.; Camino, G. Effect of clay type and loading on thermal, mechanical properties and biodegradation of poly(lactic acid) nanocomposites. *React. Funct. Polym.* **2013**, *73*, 540–549. [[CrossRef](#)]
36. Orue, A.; Eceiza, A.; Arbelaz, A. The effect of sisal fiber surface treatments, plasticizer addition and annealing process on the crystallization and the thermo-Mechanical properties of poly(lactic acid) composites. *Ind. Crop. Prod.* **2018**, *118*, 321–333. [[CrossRef](#)]
37. Mngomezulu, M.E.; Luyt, A.S.; John, M.J. Morphology, thermal and dynamic mechanical properties of poly(lactic acid)/expandable graphite (PLA/EG) flame retardant composites. *J. Thermoplast. Compos.* **2019**, *32*, 89–107. [[CrossRef](#)]
38. Shi, Y.Q.; Liu, C.; Liu, L.; Fu, L.B.; Yu, B.; Lv, Y.C.; Yang, F.Q.; Song, P.A. Strengthening, toughing and thermally stable ultra-Thin MXene nanosheets/polypropylene nanocomposites via nanoconfinement. *Chem. Eng. J.* **2019**, *378*, 122267. [[CrossRef](#)]

39. Lin, B.; Yuen, A.C.Y.; Li, A.; Zhang, Y.; Chen, T.B.Y.; Yu, B.; Lee, E.W.M.; Peng, S.H.; Yang, W.; Lu, H.D.; et al. MXene/chitosan nanocoating for flexible polyurethane foam towards remarkable fire hazards reductions. *J. Hazard. Mater.* **2020**, *381*, 120952. [[CrossRef](#)]
40. Yu, B.; Tawiah, B.; Wang, L.Q.; Yuen, A.C.Y.; Zhang, Z.C.; Shen, L.L.; Lin, B.; Fei, B.; Yang, W.; Li, A.; et al. Interface decoration of exfoliated MXene ultra-thin nanosheets for fire and smoke suppressions of thermoplastic polyurethane elastomer. *J. Hazard. Mater.* **2019**, *374*, 110–119. [[CrossRef](#)]
41. Yu, B.; Xing, W.Y.; Guo, W.W.; Qiu, S.L.; Wang, X.; Lo, S.M.; Hu, Y. Thermal exfoliation of hexagonal boron nitride for effective enhancements on thermal stability, flame retardancy and smoke suppression of epoxy resin nanocomposites via sol-gel process. *J. Mater. Chem. A* **2016**, *4*, 7330–7340. [[CrossRef](#)]
42. Cao, X.W.; Chi, X.N.; Deng, X.Q.; Liu, T.; Yu, B.; Wang, B.; Yuen, A.C.Y.; Wu, W.; Li, R.K.Y. Synergistic effect of flame retardants and graphitic carbon nitride on flame retardancy of polylactide composites. *Polym. Advan. Technol.* **2020**. [[CrossRef](#)]
43. Wu, W.; He, H.B.; Liu, T.; Wei, R.C.; Cao, X.W.; Sun, Q.J.; Venkatesh, S.; Yuen, R.K.K.; Roy, V.A.L.; Li, R.K.Y. Synergetic enhancement on flame retardancy by melamine phosphate modified lignin in rice husk ash filled P34HB biocomposites. *Compos. Sci. Technol.* **2018**, *168*, 246–254. [[CrossRef](#)]
44. Ye, X.M.; Zhang, W.C.; Yang, R.J.; He, J.Y.; Li, J.R.; Zhao, F.Q. Facile synthesis of lithium containing polyhedral oligomeric phenyl silsesquioxane and its superior performance in transparency, smoke suppression and flame retardancy of epoxy resin. *Compos. Sci. Technol.* **2020**, *189*, 108004. [[CrossRef](#)]
45. Yang, W.; Yang, W.J.; Tawiah, B.; Zhang, Y.; Wang, L.L.; Zhu, S.E.; Chen, T.B.Y.; Yuen, A.C.Y.; Yu, B.; Liu, Y.F.; et al. Synthesis of anhydrous manganese hypophosphite microtubes for simultaneous flame retardant and mechanical enhancement on poly(lactic acid). *Compos. Sci. Technol.* **2018**, *164*, 44–50. [[CrossRef](#)]
46. Tawiah, B.; Yu, B.; Yuen, A.C.Y.; Yuen, R.K.K.; Xin, J.H.; Fei, B. Thermal, crystalline and mechanical properties of flame retarded Poly (lactic acid) with a PBO-like small molecule-Phenylphosphonic Bis (2-aminobenzothiazole). *Polym. Degrad. Stabil.* **2019**, *163*, 76–86. [[CrossRef](#)]
47. Gong, K.L.; Zhou, K.Q.; Yu, B. Superior thermal and fire safety performances of epoxy-based composites with phosphorus-doped cerium oxide nanosheets. *Appl. Surf. Sci.* **2020**, *504*, 144314. [[CrossRef](#)]
48. Nine, M.J.; Tran, D.N.H.; Tung, T.T.; Kabiri, S.; Losic, D. Graphene-Borate as an efficient fire retardant for cellulosic materials with multiple and synergetic modes of action. *ACS Appl. Mater. Inter.* **2017**, *9*, 10160–10168. [[CrossRef](#)]
49. Nine, M.J.; Tran, D.N.H.; ElMekawy, A.; Losic, D. Interlayer growth of borates for highly adhesive graphene coatings with enhanced abrasion resistance, fire-retardant and antibacterial ability. *Carbon* **2017**, *117*, 252–262. [[CrossRef](#)]
50. Yuan, Y.; Yu, B.; Shi, Y.Q.; Ma, C.; Song, L.; Hu, W.Z.; Hu, Y. Highly efficient catalysts for reducing toxic gases generation change with temperature of rigid polyurethane foam nanocomposites: A comparative investigation. *Compos. Part A Appl. S.* **2018**, *112*, 142–154. [[CrossRef](#)]
51. Mu, X.W.; Pan, Y.; Ma, C.; Zhan, J.; Song, L. Novel Co₃O₄/covalent organic frameworks nanohybrids for conferring enhanced flame retardancy, smoke and CO suppression and thermal stability to polypropylene. *Mater. Chem. Phys.* **2018**, *215*, 20–30. [[CrossRef](#)]
52. Ren, Y.J.; Zhang, Y.F.; Fang, H.M.; Ding, T.P.; Li, J.L.; Bai, S.L. Simultaneous enhancement on thermal and mechanical properties of polypropylene composites filled with graphite platelets and graphene sheets. *Compos. Part A Appl. S.* **2018**, *112*, 57–63. [[CrossRef](#)]
53. Zhao, H.; She, W.; Shi, D.; Wu, W.; Zhang, Q.C.; Li, R.K.Y. Polyurethane/POSS nanocomposites for superior hydrophobicity and high ductility. *Compos. Part B Eng.* **2019**, *177*, 107441. [[CrossRef](#)]

